RSC Advances

PAPER

View Article Online
View Journal | View Issue

Cite this: *RSC Adv.*, 2017, **7**, 31671

Feasibility of USPIOs for T_1-weighted MR molecular imaging of tumor receptors†

Zhetao Liu,[ad] Jiali Cai,[b] Huilan Su,[c] Jingxing Yang,[a] Wenshe Sun,[a] Yongjie Ma,[a] Shiyuan Liu*[b] and Chunfu Zhang *[ad]

Received 2nd May 2017
Accepted 15th June 2017

DOI: 10.1039/c7ra04903j

rsc.li/rsc-advances

Ultrasmall superparamagnetic iron oxide (USPIO) nanoparticles have been extensively explored for T_2- and T_1-weighted magnetic resonance imaging (MRI). However, whether USPIOs could be simultaneously used for T_2- and T_1-weighted MR tumor receptor imaging is seldom reported. Therefore, in the current study, SPECT/MRI dual-functional probes targeting $\alpha_v\beta_3$ integrin receptors was developed based on USPIOs to examine the feasibility of T_2- and T_1-weighted dual MRI of tumor receptors. The probes were around 4.5 nm, had superior T_1 and T_2 MRI contrast effects in water suspensions and high specificity for $\alpha_v\beta_3$ integrin. After being incubated with $\alpha_v\beta_3$ positive tumor cells, MR imaging of cell suspensions indicated that the T_2 contrast effect of the probe was pronounced and enhanced compared to that in water suspensions at the same concentration, while the T_1 contrast effect vanished. After being intravenously administered into tumor bearing mice, the probes could specifically accumulate in tumors as revealed by SPECT/CT imaging. T_2-Weighted MRI showed a hypo-intense signal in the tumor region and the signal intensity enhanced with prolongation of time, while for T_1-weighted MRI, no hyper-intense signal was observed in the same tumor area. Transmission electron microscopy of tumor tissues revealed that the probes aggregated in cell organelles after targeting $\alpha_v\beta_3$ integrin. Our study suggested that USPIOs with both superior T_1 and T_2 contrast effects could only be used for T_2-weighted, but not for T_1-weighted MR tumor receptor imaging due to aggregation of the particles in cell organelles.

1. Introduction

Superparamagnetic iron oxide (SPIO) nanoparticles are conventionally used as MRI T_2 contrast agents, producing negative contrast in T_2-weighted images due to the magnetic inhomogeneity induced by their strong magnetic moment.[1,2] Because of their high sensitivity and biocompatibility, dextran-coated SPIOs, *i.e.* Feridex, have been approved by the FDA for diagnosis of liver focal lesions using MRI.[3,4] In recent years, SPIOs have also been extensively explored for theranostics of cancers.[1,5,6] For example, monoclonal antibodies, peptides and aptamers specific for different antigens have been attached to SPIOs for tumor detection and therapy. Their efficacies have been established in *ex vivo* and animal studies.[7–9] However, the intrinsic dark signal in a T_2-weighted MR image may mislead diagnosis because lesions or tumors labelled with T_2 agents could be confused with other hypo-intense areas such as bleeding, calcification or metal deposition.[10,11] Moreover, the susceptibility artefacts distort the background image. For these reasons, T_1 contrast agents are more desirable than T_2 agents for accurate high-resolution imaging.

Paramagnetic compounds with a large number of unpaired electrons, including Gd^{3+}, Mn^{2+} and Fe^{3+}, are usually used for T_1 contrast agents. T_1 contrast effect is induced by the interactions between protons of water molecules and electron spins of the metal ions.[12] Currently, the majority of T_1 contrast agents are gadolinium complex such as Gd-DTPA. This kind of contrast agent is limited by their nonspecificity to target, quick removal by renal excretion and relatively low sensitivity.[13] Early attempts to create targeted T_1-weighted molecular imaging agents with this complex to characterize tissues based on the presence of pathognomonic biosignatures initially failed because the payload of metal per homing unit (*e.g.*, antibody) reaching the target site was inadequate to produce detectable signal amplification. As a result, nano formulations with high gadolinium surface payloads were frequently prepared and intensively explored for T_1-weighted MR molecular imaging.[12,14,15] However, it has been found that gadolinium contrast agents have long-term toxicity and have the risk of inducing nephrogenic

[a]*State Key Laboratory of Oncogenes and Related Genes, Shanghai Cancer Institute, School of Biomedical Engineering, Shanghai Jiao Tong University, Shanghai 200030, China. E-mail: cfzhang@sjtu.edu.cn*

[b]*Changzheng Hospital, Secondary Military Medical University, Shanghai 200003, China. E-mail: cjr.liushiyuan@vip.163.com*

[c]*State Key Laboratory of Metal Matrix Composites, Shanghai Jiao Tong University, Shanghai 200240, China*

[d]*Department of Nuclear Medicine, Rui Jin Hospital, School of Medicine, Shanghai Jiao Tong University, Shanghai 200025, China*

† Electronic supplementary information (ESI) available. See DOI: 10.1039/c7ra04903j

system fibrosis (NSF) in patients with impaired kidney function, especially in older patients.[16] Therefore, T_1 MRI contrast agents with high sensitivity and biocompatibility are more desirable.

Iron oxides are more biocompatible than Gd-based materials because the iron species are rich in human blood,[17] which are mostly stored as ferritin in the body. SPIOs with different formulations have been proved by FDA for diagnosis and therapy of diseases.[3] For example, ferumoxytol, a carboxylized dextran-coated SPIOs, has been approved for treatment of iron-deficiency anaemia in adults with chronic kidney disease in 2009 as Feraheme. The application dose is 510 mg.[18] However, the commonly used SPIOs are not appropriate for T_1 MRI contrast agents due to their low r_1 value and large r_2/r_1 ratio, a defining parameter indicating whether the contrast agent can be employed as a positive or negative agent.[19] However, the magnetic property of SPIOs is strongly dependent on their size.[5,20] When the size of SPIOs decreases, the magnetic moment of the particles declines rapidly due to the reduction in the volume magnetic anisotropy and spin disorders on the surface of the nanoparticles,[21] whereas iron ions with 5 (Fe^{3+}) or 6 (Fe^{2+}) unpaired electrons exposed on the particle surface are increased, which is very beneficial to suppress the T_2 effect and maximize the T_1 contrast effect.[22] It has been suggested that a core size of approximately 5 nm is optimal to form a T_1 contrast agent based on iron oxide nanoparticles.[23] Ultrasmall superparamagnetic iron oxide nanoparticles (USPIOs) have been demonstrated a good T_1 MRI contrast agent.[24–26] Kim *et al.* have synthesized extremely small-sized iron oxide nanoparticles (ESIONs) of less than 4 nm and demonstrated the ESIONs had a great potential as T_1 MRI contrast agent in clinical settings.[27] Recently, we have developed a novel approach to produce polyacrylic acid (PAA) coated USPIOs (PAA@USPIOs) in large scale.[28] The PAA@USPIOs (around 4.5 nm) have a superior T_1 contrast effect and are highly effective for MRI angiography. However, whether USPIOs with good T_1 contrast effect could be used for receptor-targeted, T_1-weighted MR molecular imaging is still unknown and few works have been performed in this regard.

Therefore, in this study, we prepared a $\alpha_v\beta_3$ integrin-targeted SPECT/MRI dual functional probe (RGD-^{99m}Tc-PAA@USPIOs) based on PAA@USPIOs developed previously and evaluated its performance for T_1- and T_2-weighted dual MR tumor receptor imaging. We found that the probes have good T_1 and T_2 contrast effect in water suspensions; however, after targeting $\alpha_v\beta_3$ integrin, the T_1 contrast effect vanished and the probes only demonstrated T_2 contrast effect.

2. Experimental section

2.1 Preparation of RGD peptide-conjugated, ^{99m}Tc-labeled USPIOs probe (RGD-^{99m}Tc-PAA@USPIOs)

USPIOs coated with polyacrylic acid (PAA@USPIOs) were synthesized *via* a polyol method according to our previous reports.[28] For preparation of RGD-^{99m}Tc-PAA@USPIOs, PAA@USPIOs were first modified with ethylene diamine. Specifically, PAA@USPIOs (4.5 mg) and ethylene diamine (13.5 mg) were mixed into 2-(*N*-morpholino)ethanesulfonic acid (MES) buffer (3 mL, pH = 4.5). After adjusting the pH to 5.5, *N*-(3-dimethylaminopropyl)-*N*′-ethylcarbodiimide hydrochloridecrystalline (EDC, 20 mg) was then added and the mixture was stirred for 3 h at room temperature. Ethylene diamine modified PAA@USPIOs was retrieved by ultrafiltration (Millipore, MWCO 100 000) and washed with phosphate buffer saline (PBS, pH = 8.5) three times. To couple RGD peptide and label ^{99m}Tc, ethylene diamine derivatized USPIOs were further modified with maleimide-PEG-succinimidyl valerate (MAL-PEG-SVA) and diethylenetriaminepentaacetic acid (DTPA) dianhydride simultaneously. In detail, the aminated USPIOs (5 mg) were dispersed into 0.5 mL of PBS (pH = 8.5), into which MAL-PEG-SVA (MW = 3400, 6.0 mg) and DTPA dianhydride ($C_{14}H_{19}N_3O_8$, MW = 357.32, 0.6 mg) were added and the mixture was stirred for about 30 min at room temperature. Subsequently, the USPIOs were collected by ultrafiltration (Millipore, MWCO 100 000), washed with PBS (pH = 7.4) three times, and finally suspended into 0.5 mL of PBS (pH = 7.4). For RGD peptide conjugation, cyclic RGD peptide c(RGDyC) (abbreviated RGD, 0.3 mg) was added into the above suspensions and gently stirred overnight at room temperature. The RGD-conjugated USPIOs were ultrafiltrated (Millipore, MWCO 100 000), washed with PBS (pH = 7.4), and eventually dispersed into 0.5 mL of PBS (pH = 7.4). The peptide conjugation efficiency was determined with the Ellman method by measuring the free sulfhydryl groups in the peptide in the reaction media before and after conjugation spectrophotometrically.[29,30]

For ^{99m}Tc labeling, 2 mg of RGD peptide-conjugated USPIOs were dispersed into a mixture of ammonium acetate (90 μL, 0.25 M) and tartrate buffer (30 μL, 50 mM), then 10 μL of freshly prepared stannous chloride dihydrate solution (4 mg mL^{-1} in tartrate buffer) was added, followed by 200 μL ^{99m}Tc-pertechnetate generator eluate (2 mCi). The mixture was vortexed for about 30 min at room temperature. The labeled USPIOs were retrieved by ultrafiltration and washed with PBS (pH = 7.4) three times.[31,32]

^{99m}Tc radiolabeling efficiency and its stability on the probe were evaluated by radio-thin layer chromatography (AR2000, Bioscan, Washington, USA) using acetone as the mobile phase. In this system, ^{99m}Tc-labeled USPIOs remain at the origin, while ^{99m}Tc-pertechnetate migrates to retardation factor (R_f) = 0.7–0.9. The labeling efficiency was calculated by dividing the radioactivity retained at the origin to the total radioactivity added. To assess the radiochemical stability of ^{99m}Tc in the physiological condition, the probe RGD-^{99m}Tc-PAA@USPIOs was co-incubated with 200 μL of fresh mouse plasma at 37 °C for different periods of time. Stability of ^{99m}Tc was expressed as a percentage of radioactivities retained on the particles to the radioactivity of the probes.[33]

In addition, RGD peptide-conjugated, technetium (Tc)-labeled USPIOs (RGD-Tc-PAA@USPIOs) were also prepared as a "cold" probe using $NaTcO_4$ as a precursor under the same conditions as those for ^{99m}Tc labeling. At the same time, scramble peptide c(RADyC) (abbreviated RAD) conjugated-, ^{99m}Tc- or Tc-labeled PAA@USPIOs were also prepared as control probes (RAD-^{99m}Tc-PAA@USPIOs, RAD-Tc-PAA@USPIOs).

2.2 Characterizations of the probes

The morphology and core size of the probes were investigated by transmission electron microscopy (TEM, JEOL2010) at an accelerating voltage of 200 kV. The average core size was determined by measuring the diameters of more than 100 particles in the TEM images using ImageJ analysis software (NIH). The hydrodynamic sizes and zeta potentials were analysed by using a dynamic light scattering (DLS) instrument (NanoZS, Malvern, UK). The T_1 and T_2 relaxation times were determined using a 1.41 T (60 MHz) Bruker mq60 nuclear magnetic resonance analyzer (Bruker, Karlsruhe, Germany) at 37 °C. For this purpose, the probes were diluted in a series of concentration, which were measured using an atomic absorption spectrophotometer (AAS, Z-2000, Hitachi, Japan). Inversion recovery and multi-echo CPMG sequences were used to determine the T_1 and T_2 relaxation times of the probe samples, and thus calculate the R_1 ($1/T_1$) and R_2 ($1/T_2$) relaxation rates of each sample. The R_1 and R_2 were plotted against probe concentration (mM, in iron) to respectively determine the longitudinal (r_1) and transverse (r_2) relaxivities from the slope of the linear fit. The T_1 and T_2 relaxation times and thus the r_1 and r_2 relaxivities were also determined using a 3 T clinical MRI scanner (TrioTim, Siemens, Germany) at the room temperature. The measurement setup and imaging parameters were detailed in ESI.† To study the effect of surface modifications on MRI property of the USPIOs, relaxivities of the particles at each step of probe preparation were evaluated.

2.3 MRI of RGD-Tc-PAA@USPIOs suspensions

To evaluate the MRI performance of the probe, RGD-Tc-PAA@USPIOs was diluted in deionized water in plastic vials. To avoid susceptibility artefacts from the surrounding air in the scans, all the samples were placed in a water-containing plastic container at room temperature. MRI was performed with a 3 T MRI scanner (TrioTim, Siemens, Germany) using a clinical head coil with T_1- (TR = 500 ms, TE = 15 ms, average 3, FOV = 100 mm, matrix = 192 × 192, slice thickness = 2 mm) and T_2-weighted spin-echo sequence (TR = 2000 ms, TE = 37 ms, average 3, FOV = 100 mm, matrix = 192 × 192, slice thickness = 2 mm).

2.4 Cytotoxicity assay

H1299 cells, a non-small lung cancer cell line, were provided by Shanghai Institutes for Biological Sciences, CAS (Shanghai, China), grown in DMEM medium supplemented with 10% FBS, and maintained at 37 °C under a humidified atmosphere containing 5% CO_2. Cytotoxicity of the probes was evaluated by the typical 3-(4,5-dimethylthiazol-2-yl)-2,5-diphenyltetrazolium bromide (MTT) reduction assays using the cold probe (RGD-Tc-PAA@Fe_3O_4).[33,34] For this purpose, the cells were seeded in a 96-well plate with 1×10^4 cells per well and cultured with the media containing various concentrations of probes (0.15, 0.5 and 1.5 mM in iron) for different period of time. After incubation, the culture media were removed and the cells were washed with PBS (pH 7.4) three times. Subsequently, 100 μL aliquots of MTT solution were added. After incubation for another 4 h, the media were replaced with 100 μL of dimethyl sulfoxide per well, and the absorbance was monitored by a microplate reader at a wavelength of 490 nm. The cell viability was expressed as the percentage of absorbance of the cells incubated with the probes to that of the cells maintained in a normal culture medium.

2.5 *In vitro* cell binding and specificity

H1299 cells, a non small-lung cancer cell line, overexpresses $\alpha_v\beta_3$ integrin.[35] Specificity of the probes for $\alpha_v\beta_3$ integrin was examined by Prussian blue staining and AAS quantifications of intracellular iron contents of the cells treated with the probes. For Prussian blue staining, H1299 cells were seeded on glass coverslips and cultured in six-well plates with media containing RGD-Tc-PAA@USPIOs, RAD-Tc-PAA@USPIOs or RGD-Tc-PAA@USPIOs plus free RGD peptide (10 μM) at the concentration of 0.5 mM (in iron) for 1 h. After incubation, the cells were washed with PBS (0.1 M, pH 7.4) three times and then fixed with paraformaldehyde (4%). The fixed cells were stained with 10% Prussian blue for 5 min, a mixture of 10% Prussian blue and 20% HCl (1 : 1) for 30 min, and nuclear fast red for 5 min successively. Slides were examined by optical microscopy using a Leica DMLB microscope (Leica Microsystems Inc, Buffalo Grove, Illinois). For quantifications of intracellular iron content, the cells (3×10^6) were collected and digested with aqua regia at 60 °C for 1 h, and then the intracellular iron content was determined by AAS.

2.6 MR cell imaging

After treated with the probes, the cells (1×10^6) were homogenously suspended in gelatin (2%, 500 μL) in plastic vials and placed in a water tank. T_1- and T_2-weighted MRI was performed with a 3 T MRI scanner (TrioTim, Siemens, Germany) using the same parameters as those for probe imaging aforementioned. In addition, MR imaging of RGD-Tc-PAA@USPIOs-treated cells suspended in gelatin at different concentrations (in iron) was also performed.

2.7 SPECT/CT and MR imaging

All experiments were performed in compliance with the National Regulations for the Administration of Affairs Concerning Experimental Animals and approved by the animal protection and care committee of Shanghai Jiao Tong University. H1299 tumor xenograft was conducted by implanting tumor cells (1×10^6) under the left limb of BALB/c mice (Slaccas, Shanghai, China). Tumors were allowed to grow over the next 3–4 weeks. For SPECT/CT imaging, tumor-bearing mice (five mice per group) were intravenously injected with RGD-^{99m}Tc-PAA@USPIOs, RAD-^{99m}Tc-PAA@USPIOs, or RGD-^{99m}Tc-PAA@USPIOs plus free RGD peptide (0.15 mM, 100 μL) at the radioactive dose of 3.7 MBq. SPECT/CT scans were performed at 0.5, 1, 3, 6 h post probe injection using a small-animal imaging system (Bioscan, Washington, USA) and the images were obtained at 32 projections over 360 °C (radius of rotation = 7.6 cm, 30 s per projection). The CT images were used to provide anatomical references to the tumor location.

Reconstructed data from SPECT and CT were visualized and co-registered using InVivoScope provided by the manufacturer.

After SPECT/CT imaging, the mice were euthanized and dissected. The major organs (tumor, heart, liver, spleen, lung, kidney, stomach, intestine, brain, bone, pancreas, bladder, muscle) were harvested and weighed. The radioactivity associated with each organ was determined by a γ-counter along with 3×0.5 mL aliquots of the diluted standard representing 100% of the injected dose. The mean activities were used to obtain the percentage of injected dose per gram of tissue (% ID per g).

MR imaging of tumors was performed using the cold probe. H1299 tumor bearing mice (five mice per group) were treated with RGD-Tc-PAA@USPIOs, RAD-Tc-PAA@USPIOs, or RGD-Tc-PAA@USPIOs plus free RGD (0.15 mM, 100 μL) at the dose of 100 μmol Fe per kg bodyweight.[34] MR imaging was conducted using a 3 T MRI scanner (Signa Excite HDx, GE, Milwaukee, Wisconsin) equipped with a customized coil. For image acquisition and determination of T_1 and T_2 relaxation times of tumors before and after probe injection, T_1 mapping sequence ($T_R = 3000$ ms, $T_E = 15$ ms, and inversion delays of 500, 1000, 1500, 2000, 2500, 3000, and 3500 ms) and T_2 mapping sequence ($T_R = 3000$ ms, $T_E = 20$–160 ms, 8 echo, matrix $= 128 \times 128$, FOV = 150 mm, slice thickness = 2 mm) were utilized.

2.8 Histological studies

After MR imaging, the mice were euthanized. The tumors were removed, imbedded in OCT glue (Sakura Finetek Inc, Torrance, California) and then frozen with nitrogen. 10 μm sections were made using a cryotome (CM1850; Leica Microsystems GmbH). The sections were first fixed in acetone for 10 min at 4 °C and then air-dried for 30 min.

To verify RGD-Tc-PAA@USPIOs targeting tumor angiogenic vessels, Prussian staining was performed. The procedure for the tissue staining was same as that for cell staining. The slides were examined by optical microscopy using a Leica DMLB microscope (Leica Microsystems Inc, Buffalo Grove, Illinois).

To identify the conditions of the probes in tumors, TEM examinations of tumor tissues were conducted. The procedure for the sample preparation was same as that for cells described previously. Micrographs were taken with TEM operating at an acceleration voltage of 80 kV (Philip CM-120, Eindhoven, The Netherlands).

To identify the expression of $\alpha_v\beta_3$ integrin, immunohistological staining of tumor tissues against $\alpha_v\beta_3$ integrin was performed. To this end, the sections were treated with a primary rat-anti-mouse CD61 monoclonal antibody (1 : 50 dilution; BD Biosciences) and a biotinylated goat-anti-rat IgG (BD Bioscience) in combination with streptavidin-horseradish peroxidase (HRP) and the DAB detection system. The tumor sections were counterstained with hematoxylin and returned to blue by using an ammonia solution. In addition, tumor vessels were also stained against CD31.

2.9 Statistical evaluation

All data were presented as means ± standard deviations (SD). Statistical analysis of intracellular iron content (AAS data) and biodistributions of the probes were conducted by using a Wilcoxon rank sum test. A p value of <0.05 was considered to indicate significant differences between groups.

3. Results and discussion

3.1 Synthesis and characterizations of RGD-^{99m}Tc-PAA@USPIOs

PAA@USPIOs was prepared by polyol method in the presence of PAA. The TEM size and zeta potential of PAA@USPIOs were 4.5 ± 0.5 nm and −55 mV, respectively. The longitudinal (r_1) and transversal (r_2) relaxivities were 8.67 and 25.36 mM^{-1} s^{-1}, with

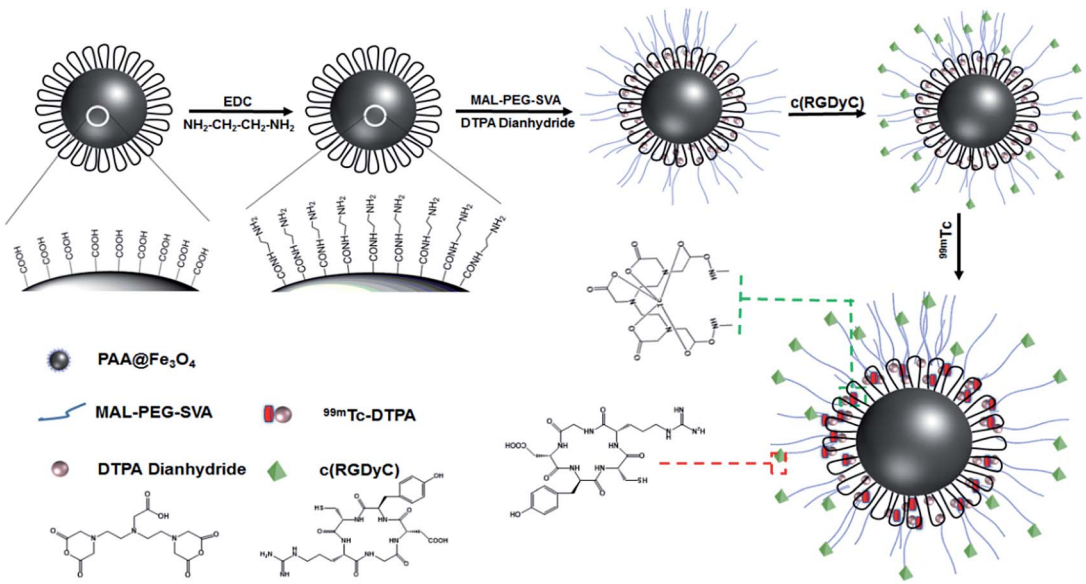

Scheme 1 Schematic diagram of the procedure for fabrication of the RGD-^{99m}Tc-PAA@USPIOs probe.

r_2/r_1 ratio of 2.93. PAA@USPIOs was highly effective for MRI angiography. To conjugate RGD peptides and label ^{99m}Tc, PAA@USPIOs was first modified with ethylene diamine. After the modification, zeta potential of the USPIOs raised to −28 mV. Then, the aminated PAA@USPIOs was further derivatized by MAL-PEG-SVA and diethylene triamine pentaacetic acid (DTPA) dianhydride simultaneously. Both of the substances could form covalent bonds with the primary amine present on the aminated PAA@USPIOs through amide bonds. The RGD peptides (c(RGDyC)) were then covalently conjugated to the USPIOs through thiol–maleimide linkages between the peptide and PEG. The RGD conjugation efficiency was about 98% as measured by Ellman method. ^{99m}Tc was labeled onto the USPIOs by complexing ^{99m}Tc with DTPA.[33,36] The labeling efficiency, as verified by RTLC, was 95%. The procedure for preparation of the probe was shown in Scheme 1. Once fully labeled, the RGD-^{99m}Tc-PAA@USPIOs were purified using size exclusion filters and size exclusion chromatography with disposable columns containing Sephadex G-25 medium, using saline as the eluent. The purified RGD-^{99m}Tc-PAA@USPIOs were highly stable in mouse plasma, retaining around 95% of the initial ^{99m}Tc content after 24 h incubation at 37 °C (Fig. 1A).

We also prepared USPIOs without ^{99m}Tc for use as cold probes, labeling instead with technetium using $NaTcO_4$ as a precursor (RGD-Tc-PAA@USPIOs). The TEM size of RGD-Tc-PAA@USPIOs was 4.5 ± 1.2 nm, similar to PAA@USPIOs and the probes were well separated from each other without observable aggregation in deionized water (Fig. 1B). Zeta potential of the probes was found to be around −32 mV. In order to test the stability of the probe, we measured the hydrodynamic size of the probes in mouse serum and PBS using DLS for different periods of time. In both cases, the hydrodynamic sizes were 102 ± 2 nm and 95 ± 3 nm, respectively, and did not change significantly during 24 h (Fig. 1C). Fig. 1D showed the $1/T_1$ and $1/T_2$ relaxation rates of the probes at 1.41 T as a function of the iron concentrations. It was found that the relaxation rates varied linearly with

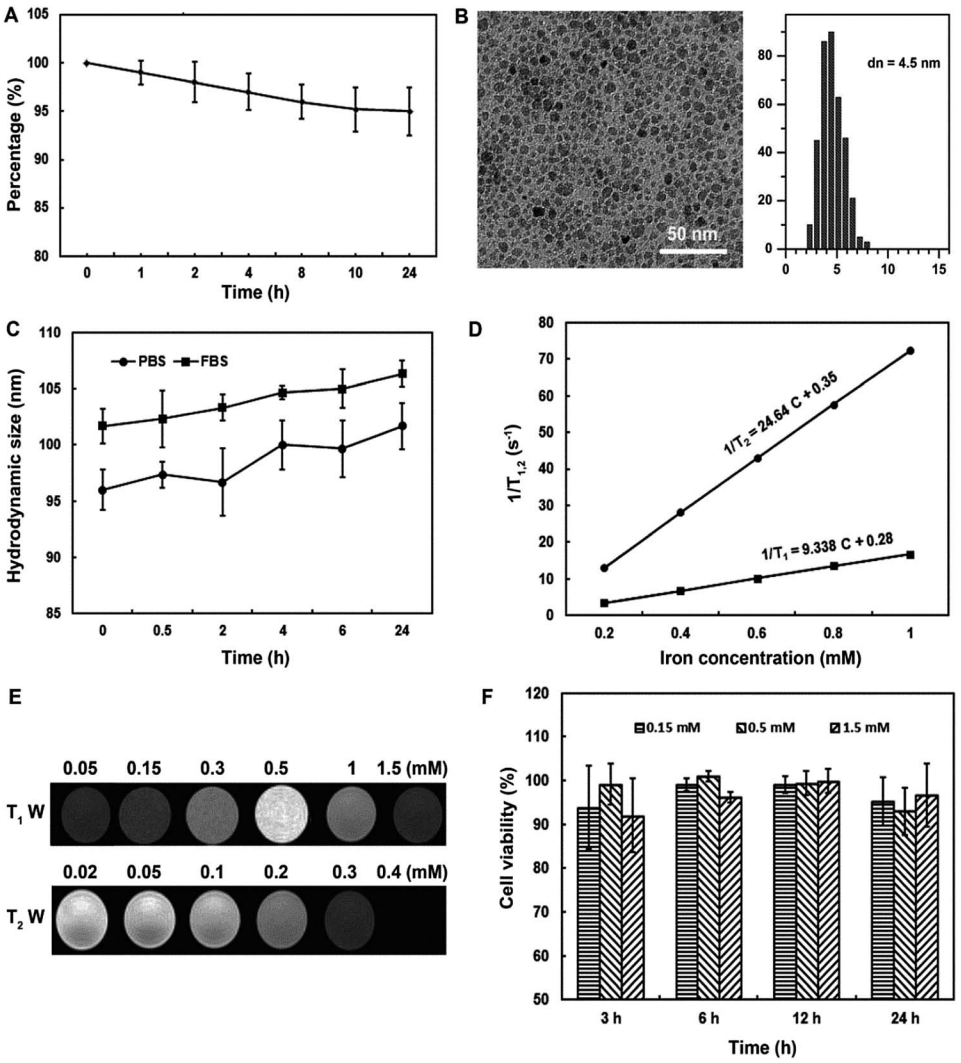

Fig. 1 Characterizations of the probes. (A) Stability of ^{99m}Tc on the probe RGD-^{99m}Tc-PAA@USPIOs incubated in mouse serum for different periods of time at 37 °C. (B) TEM image of the cold probe RGD-Tc-PAA@USPIOs (left) and its size distribution (right). (C, D) Stability and MRI properties of the cold probe. (E) T_1 and T_2-weighted MRI of the probe water suspensions. (F) Cytotoxicity of the cold probes.

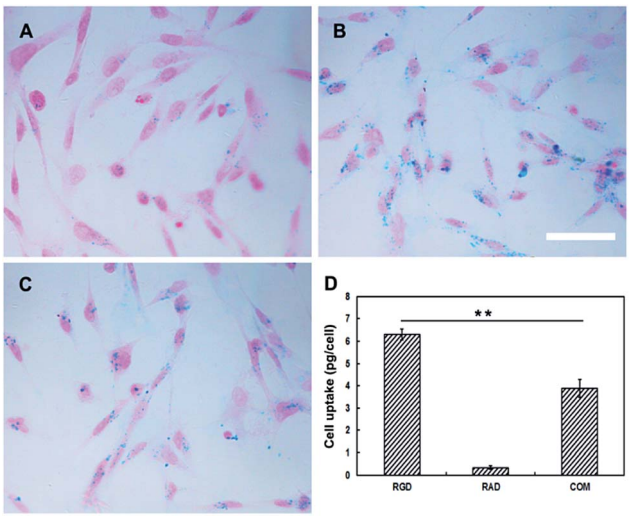

Fig. 2 Specificity of the probe RGD-Tc-PAA@USPIOs for $\alpha_v\beta_3$ integrin. (A–C) Prussian blue staining of H1299 cells incubated with control probe RAD-Tc-PAA@USPIOs (A), RGD-Tc-PAA@USPIOs (B) and RGD-Tc-PAA@USPIOs plus free RGD peptide (10 μM) (C). (D) AAS quantification of intracellular iron content. $^{**}p < 0.01$.

the iron concentrations. The longitudinal (r_1) and transversal (r_2) relaxivities were 9.34 mM^{-1} s^{-1} and 24.64 mM^{-1} s^{-1}, respectively, with r_2/r_1 ratio of 2.64, better than other clinically approved USPIOs-based T_1 contrast agent.[1] Moreover, after each step of surface modification, both the longitudinal and transverse relaxivities of the particles were similar to those of PAA@USPIOs, indicating that the surface modifications did not significantly affect the relaxation properties of the particles (Table S1†). However, consistent with previous reports, the r_2 relaxivity increased, while the r_1 decreased at a higher magnetic field (3 T, Table S1†).[37]

To investigate the MR signal enhancement effects, the aqueous solutions of RGD-Tc-PAA@USPIOs at different concentrations (in iron) were measured on a clinical 3 T MRI scanner. As shown in Fig. 1E, RGD-Tc-PAA@USPIOs induced a dark signal on the T_2-weighted images and a bright signal on the T_1-weighted images, in line with other USPIOs contrast agents.[38] The T_2 signal intensity decreased in a concentration-dependent manner.[39] However, T_1-weighted images showed an increasing enhancement with a marked brightening until a given iron concentration, but for higher concentrations the signal decreased and darkening was observed. Our results were consistent with previous observations, and the phenomenon might arise from overdose effects.[40] The overdose effect is attributed to increasing T_2 shortening at higher doses, which reduces the signal intensity and cancel out the signal-enhancing effect of T_1 shortening even at the short echo times used.[41]

3.2 Cytotoxicity of the probes

Cytotoxicity of the probes was evaluated *in vitro* with MTT reduction assay. H1299 cells were incubated with RGD-Tc-

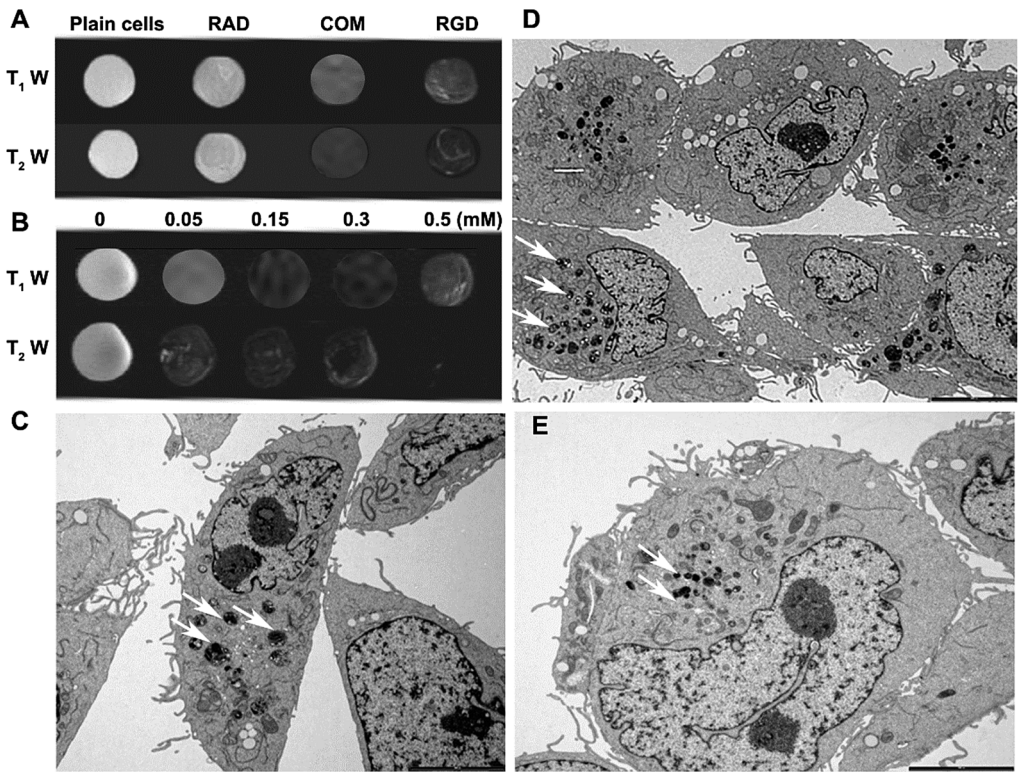

Fig. 3 MRI of cell suspensions and the physical status of RGD-Tc-PAA@USPIOs in cells. (A) T_1 and T_2-weighted MRI of cells incubated with control probe RAD-Tc-PAA@USPIOs (RAD), RGD-Tc-PAA@USPIOs (RGD) and RGD-Tc-PAA@USPIOs plus free RGD peptide (10 μM, COM). (B) T_1 and T_2-weighted MRI of cells incubated with RGD-Tc-PAA@USPIOs at different concentrations (in iron). (C–E) TEM images of cells treated with control probe RAD-Tc-PAA@USPIOs (C), RGD-Tc-PAA@USPIOs (D) or RGD-Tc-PAA@USPIOs plus free RGD peptide (10 μM) (E). Bar: 5 μm.

PAA@USPIOs at different concentrations (0.15, 0.5, 1.5 mM in iron) for different period of time (3, 6, 12, 24 h) (Fig. 1F). The results indicated that the viability of the cells was not affected by the presence of the probes even up to 1.5 mM for 24 h (~95%), suggesting that similar to PAA@USPIOs demonstrated previously;[28] our probes were noncytotoxic and safe for further *in vivo* use.[42] This result also indicated that the surface modifications did not alter the safety profile of the USPIOs.

3.3 Specificity of the probes

To evaluate the specificity of the probes for $\alpha_v\beta_3$, H1299 cells were cultured with media containing RGD-Tc-PAA@USPIOs, RAD-Tc-PAA@USPIOs, or RGD-Tc-PAA@USPIOs plus free RGD peptide (10 μM) at the concentration of 0.5 mM (in iron) for 1 h. Prussian blue staining revealed that cell uptake of RGD-Tc-PAA@USPIOs was greater than that of RAD-Tc-PAA@USPIOs, and the uptake was suppressed by free RGD peptide (Fig. 2A–C). Consistent with Prussian blue staining, AAS quantification indicated that cell uptake of RGD-Tc-PAA@USPIOs and RAD-Tc-PAA@USPIOs was 6.5 ± 0.2 and 0.6 ± 0.1 pg per cell, respectively, and the uptake was reduced to 3.8 ± 0.4 pg per cell after inhibition by free peptide ($p < 0.01$) (Fig. 2D). These observations suggested that RGD-Tc-PAA@USPIOs could specifically target $\alpha_v\beta_3$ integrin and the cellular uptake of the probes was mediated by the receptor.[8,36]

3.4 MRI of cell suspensions

As demonstrated previously, RGD-Tc-PAA@USPIOs was a good T_1 MRI contrast agent in relatively lower concentrations. To determine whether the probes could still act as T_1 MRI contrast agent after targeting tumor cells, MR imaging of H1299 cells (1×10^6) treated with the probes was performed. In contrast to the dispersed isolated probes in water suspensions, the signal enhancement in T_1-weighted MRI images of the probe-treated cells was negative and the signal loss was similar to that in the T_2-weighted MRI images. The dark signal intensity lessened after competition with free RGD peptide. Even for the RAD-Tc-PAA@USPIOs-treated cells, the signal intensity also decreased marginally (Fig. 3A). To exclude the possible overdose effect observed in probe water suspensions, we suspended the probe-treated cells at concentrations (in iron) same as those of probe suspensions for MRI. As shown in Fig. 3B, even at the lowest cell concentration (0.05 mM), T_1-weighted MR signal also decreased compared to that of the plain cells. Different from the dispersed isolated probes, the positive enhancement was no longer present, whereas the darkening effect increased over the whole concentration range. As observed in Prussian blue staining, $\alpha_v\beta_3$ integrin targeting induced cell uptake of the probe. Previous studies indicated that the receptor-mediated uptake would induce the probes to be accumulated and clustered in cell lysosomes.[34] Clustering would dramatically enhance the T_2 effect, while diminish the T_1 effect of USPIOs.[43,44]

To evaluate the physical status of the probes in cells, TEM examinations of the cells were performed. In line with Prussian blue staining and AAS quantification, TEM microscopies revealed that cell ingestion of RGD-Tc-PAA@USPIOs (Fig. 3D) was more than that of RAD-Tc-PAA@USPIOs (Fig. 3C) and free RGD peptide competition reduced the ingestion (Fig. 3E). Both RGD-Tc-PAA@USPIOs and RAD-Tc-PAA@USPIOs were internalized by cells and densely packed in cell lysosomes (arrowheads).[7]

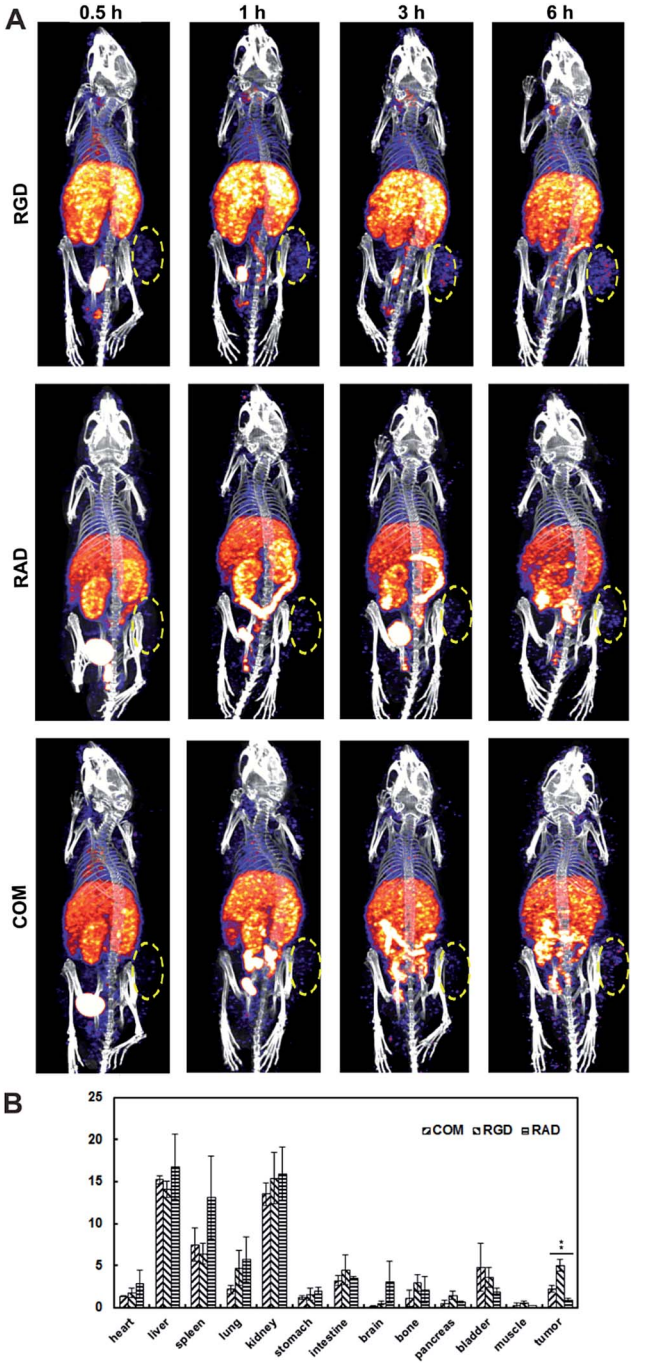

Fig. 4 Specificity of RGD-^{99m}Tc-PAA@USPIOs for tumors. (A) SPECT/CT imaging of H1299 tumor bearing mice intravenously injected with RGD-^{99m}Tc-PAA@USPIOs (RGD), RAD-^{99m}Tc-PAA@USPIOs (RAD) and RGD-Tc-PAA@USPIOs plus free RGD peptide (COM). (B) Biodistributions of the probes. $^{**}p < 0.01$.

Change of physical status from the dispersed isolated particles in a water solution to aggregations in cytoplasm may be the reason for the probe loosing MRI T_1 performance. The precondition for USPIOs used as T_1 contrast agent is that the USPIOs should have a high r_1 and a relatively lower r_2, thus lower r_2/r_1 ratio.[22,45] Clustering of USPIOs would dramatically enhance the T_2 contrast effect (r_2), while weakening the T_1-shortening effect (r_1), resulting in high r_2/r_1 ratio and limiting USPIOs to be a T_1 contrast agent.[46] Our results were actually in accordance with previous observations that intracellular confinement of magnetite nanoparticles within micrometric endosomes led to a significant decrease of the r_1 relaxivity compared to that of the dispersed isolated nanoparticles. Consequently, for T_1-weighted sequences, the signal intensity fell essentially, so the positive enhancement no longer existed.[37,47] The possible explanation was that the intracellular compartmentalization would restrict water diffusion and/or particle diffusion and thereby limited the T_1 effect of the USPIOs in cells.[37,47]

3.5 MRI and SPECT/CT imaging of tumors

To investigate the potential of the probe for T_1-weighted MR tumor receptor imaging, next, the specificity of the probe for $\alpha_v\beta_3$ integrin *in vivo* was first assessed by SPECT/CT imaging. H1299 tumor bearing mice were intravenously injected with RGD-^{99m}Tc-PAA@USPIOs, RAD-^{99m}Tc-PAA@USPIOs or RGD^{99m}Tc-PAA@USPIOs plus free RGD (3.7 MBq). SPECT/CT imaging revealed that tumor accumulation of RGD-^{99m}Tc-PAA@USPIOs was obvious 30 min post injection and augmented with the prolongation of time. Six hours post injection, strong radioactive signal was observed in tumor region. Moreover, the accumulation was greater than that of RAD-^{99m}Tc-PAA@Fe_3O_4 at each time point examined, and reduced in the presence of free RGD peptide competition (Fig. 4A). Consistent with SPECT/CT imaging, biodistribution studies indicated that tumor accumulations of RGD-^{99m}Tc-PAA@USPIOs, RAD-^{99m}Tc-PAA@USPIOs and RGD-^{99m}Tc-PAA@USPIOs plus free RGD were 4.98 ± 0.70, 0.90 ± 0.23, and 2.25 ± 0.03 ID% per g (**$p < 0.01$), respectively. These

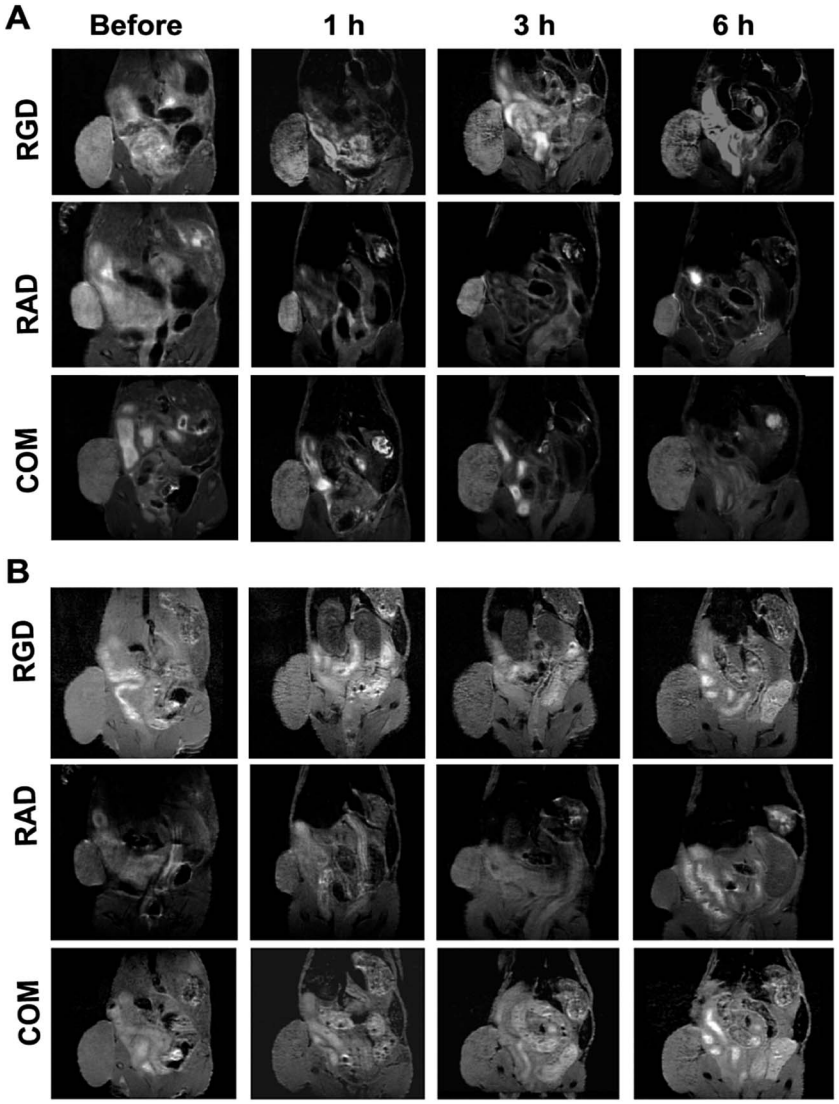

Fig. 5 (A and B) T_2- and T_1-weighted MRI of mice intravenously injected with RGD-Tc-PAA@USPIOs (RGD), control probe (RAD-Tc-PAA@USPIOs) (RAD) and RGD-Tc-PAA@USPIOs plus free RGD peptide (COM).

observations indicated that the RGD-^{99m}Tc-PAA@USPIOs specifically target $\alpha_v\beta_3$ integrin *in vivo*.[33,34]

T_2- and T_1-weighted MRI were performed using the cold probe and a 3 T MRI scanner by an alternate scanning manner. For T_2-weighted MRI, inhomogeneous dark signals were observed in tumor regions for mice receiving RGD-Tc-PAA@Fe_3O_4 probe 1 h post injection and the hypo-intense signals further decreased with the prolongation of time (Fig. 5A). Accordingly, the T_2 relaxation time changes of the tumors before and after probe injection were 28 ± 6 ms (1 h), 36 ± 5 ms (3 h) and 44 ± 8 ms (6 h), respectively. For mice treated with RGD-Tc-PAA@Fe_3O_4 plus free RGD peptide, the inhomogeneous dark signals in tumor regions could still be observed, but were less pronounced. For the control mice treated with RAD-Tc@Fe_3O_4 probes, the decrease in the MR signal intensity in the tumor regions was only marginal. These results were consistent with previous reports that iron oxide nanoparticles concentrated at the target site generated dark or negative contrast in T_2-weighted images.[48] However, for T_1-weighted MRI, no bright signals in tumor regions were observed for mice receiving RGD-Tc-PAA@Fe_3O_4 (Fig. 5B), even if the probes were present in the tumor regions as clearly observed in T_2-weighted MRI. The T_1 relaxation time changes of the tumors before and after probe injection were 6 ± 4 ms (1 h), 7 ± 5 ms (3 h) and 8 ± 2 ms (6 h), respectively. Due to the superior T_1 contrast effect of the probes, bright signals in tumor region were expected, similar as those from gadolinium-based molecular imaging probes.[10,33] Our results were actually consistent with previous report on liver MR imaging using USPIOs-based T_1 contrast agent,[49] in which T_1-weighted MRI signal intensity in liver region was first increased by 26% shortly after injection of the USPIOs and then gradually decreased, in a manner similar to that in T_2-weighted MRI. The possible reason was that shortly after injection, the USPIOs were still in blood pool of liver and can perform well as T_1 contrast agent. Once internalized by Kuffer cells in sinus hepaticus, the T_1 effect diminished due to aggregation of the particles in cytoplasm. Considering the results of MR cell imaging, we speculated that RGD-Tc-PAA@Fe_3O_4 probe may also clustered in tumor after targeting tumor cells and made them not suitable for T_1-weighted MR imaging.

USPIOs have been derivatized with varieties of biomolecules, such as peptides, aptamers and antibodies, targeting different biomarkers for MR molecular imaging of cancers.[50,51] RGD-containing peptides have high affinity to $\alpha_v\beta_3$ integrin receptor, which is overexpressed on endothelial cells during angiogenesis, but barely detectable in most normal organs.[52] Therefore, it is widely used for diagnostic imaging. In addition to targeting tumor angiogenic vessels, our probe RGD-^{99m}Tc-PAA@USPIOs could also address H1299 tumor cells after extravasation from tumor vessels. Therefore, compared to probes binding to receptors that only express on tumor cells,

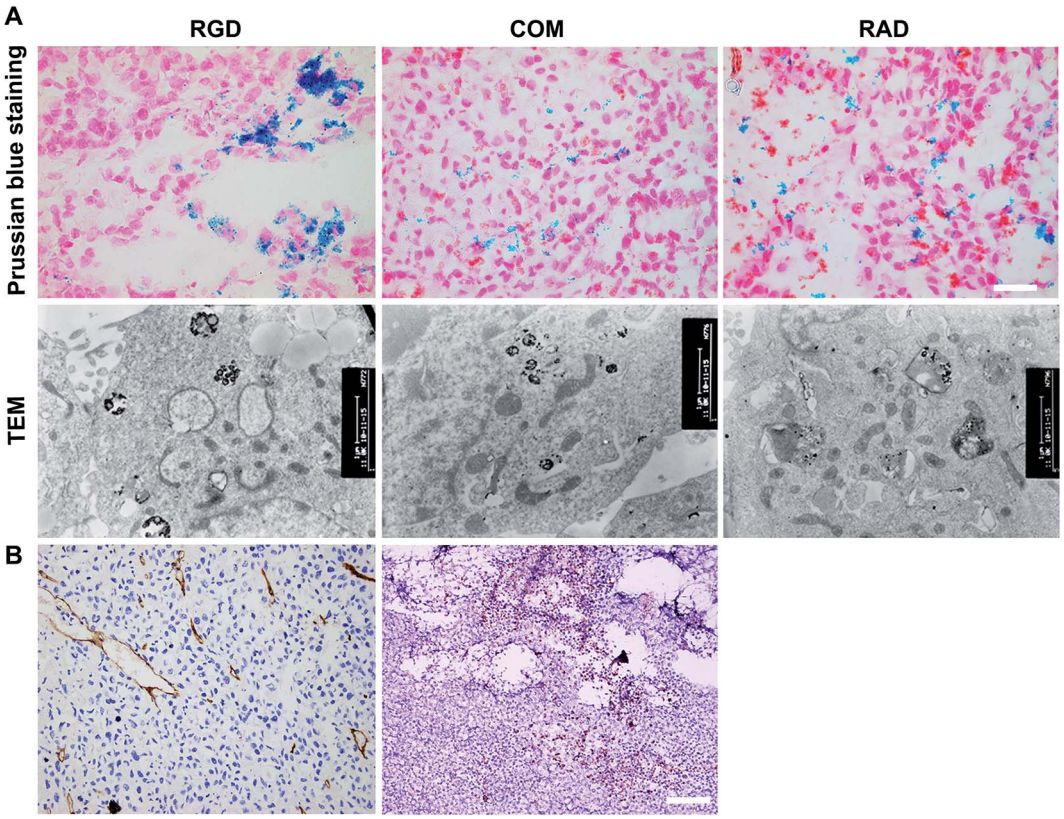

Fig. 6 Histological studies of tumor tissues. (A) Prussian blue staining (upper role) and TEM images of tumor tissues from mice receiving RGD-Tc-PAA@USPIOs (RGD), control probe RAD-Tc-PAA@USPIOs (RAD) and RGD-Tc-PAA@USPIOs plus free RGD peptide (COM) 6 h post injection. (B) Immunohistological staining of tumor tissues against CD31 (left) and CD61 (right). Scale bar: 20 μm.

the targeting efficiency and thus the detection sensitivity of our probes for H1299 tumor might be higher.

3.6 Histological studies

After MRI, the mice were sacrificed, the tumors were removed, and histological studies of the tumor tissues were performed. Microscopic examination of tumor sections stained with Prussian blue revealed that RGD-Tc-PAA@USPIOs registered the tumor angiogenic vessels (Fig. 6A) and its targeting efficiency was reduced after competition with free RGD peptide. RAD-Tc-PAA@USPIOs was also found in the tumors, though to a lesser extent, which indicated nonspecific uptake due to the enhanced permeation and retention (EPR) effect.[53] To identify the physical conditions of the probes in tumors, TEM examinations of tumor tissues were also performed (Fig. 6A). TEM microscopies showed that the probes accumulated and packed in cytoplasmic vesicles, similar as that observed in cell suspensions. Aggregation of the probes within cells may be the reason for poor T_1-weighted effect in tumors. Immunostaining of the tumor tissues against CD31 (Fig. 6B left) and CD61 (Fig. 6B right) indicated that H1299 tumors were highly vascular and some of the tumor vessels were $\alpha_v\beta_3$ positive.

4. Conclusions

In summary, we have developed a $\alpha_v\beta_3$ integrin targeted, SPECT/MRI dual functional molecular imaging probe based on USPIOs. The probes had superior T_1 and T_2 MRI contrast effects in water suspensions and high specificity for $\alpha_v\beta_3$ integrin. After targeting $\alpha_v\beta_3$ integrin, however, its performance as T_1 positive contrast agent was significantly suppressed and only T_2 contrast effect was manifested both *in vitro* and *in vivo* due to clustering of the probe in cell vesicles. Our study suggested that for MR tumor receptor imaging, USPIOs even with good T_1 contrast effect could only be used for T_2-weighted imaging.

Acknowledgements

This work was supported by the National Natural Science Foundation of China (grant 81571729, 81230030) and grants from the State Key Laboratory of Oncogenes and Related Genes (90-15-03).

Notes and references

1 N. Lee, D. Yoo, D. Ling, M. H. Cho, T. Hyeon and J. Cheon, *Chem. Rev.*, 2015, **115**, 10637–10689.
2 B. R. Smith and S. S. Gambhir, *Chem. Rev.*, 2017, **117**, 901–986.
3 A. Tanimoto and S. Kuribayashi, *Eur. J. Radiol.*, 2006, **58**, 200–216.
4 D. D. Stark, R. Weissleder, G. Elizondo, P. F. Hahn, S. Saini, L. E. Todd, J. Wittenberg and J. T. Ferrucci, *Radiology*, 1988, **168**, 297–301.
5 L. Wu, A. Mendoza-Garcia, Q. Li and S. Sun, *Chem. Rev.*, 2016, **116**, 10473–10512.
6 J. E. Rosen, L. Chan, D.-B. Shieh and F. X. Gu, *Nanomedicine: Nanotechnology, Biology and Medicine*, 2012, **8**, 275–290.
7 H. Zhu, L. Zhang, Y. Liu, Y. Zhou, K. Wang, X. Xie, L. Song, D. Wang, C. Han and Q. Chen, *Sci. Rep.*, 2016, **6**, 39245.
8 R. Misri, D. Meier, A. C. Yung, P. Kozlowski and U. O. Häfeli, *Nanomedicine: Nanotechnology, Biology and Medicine*, 2012, **8**, 1007–1016.
9 F. Ai, C. A. Ferreira, F. Chen and W. Cai, *Wiley Interdiscip. Rev.: Nanomed. Nanobiotechnol.*, 2016, **8**, 619–630.
10 H. B. Na, J. H. Lee, K. An, Y. I. Park, M. Park, I. S. Lee, D.-H. Nam, S. T. Kim, S.-H. Kim, S.-W. Kim, K.-H. Lim, K.-S. Kim, S.-O. Kim and T. Hyeon, *Angew. Chem., Int. Ed.*, 2007, **46**, 5397–5401.
11 Z. Li, B. Tan, M. Allix, A. I. Cooper and M. J. Rosseinsky, *Small*, 2008, **4**, 231–239.
12 Y.-K. Peng, S. C. E. Tsang and P.-T. Chou, *Mater. Today*, 2016, **19**, 336–348.
13 Z. Gao, T. Ma, E. Zhao, D. Docter, W. Yang, R. H. Stauber and M. Gao, *Small*, 2016, **12**, 556–576.
14 S. Ghiani, M. Capozza, C. Cabella, A. Coppo, L. Miragoli, C. Brioschi, R. Bonafè and A. Maiocchi, *Nanomedicine: Nanotechnology, Biology and Medicine*, 2017, **13**, 693–700.
15 A. H. Schmieder, P. M. Winter, T. A. Williams, J. S. Allen, G. Hu, H. Zhang, S. D. Caruthers, S. A. Wickline and G. M. Lanza, *Radiology*, 2013, **268**, 470–480.
16 P. H. Kuo, E. Kanal, A. K. Abu-Alfa and S. E. Cowper, *Radiology*, 2007, **242**, 647–649.
17 R. Chen, D. Ling, L. Zhao, S. Wang, Y. Liu, R. Bai, S. Baik, Y. Zhao, C. Chen and T. Hyeon, *ACS Nano*, 2015, **9**, 12425–12435.
18 B. Schiller, P. Bhat and A. Sharma, *Clin. Ther.*, 2014, **36**, 70–83.
19 P. A. Rink and R. N. Muller, *Eur. J. Radiol.*, 1999, **9**, 998–1004.
20 E. D. Smolensky, H.-Y. E. Park, Y. Zhou, G. A. Rolla, M. Marjanska, M. Botta and V. C. Pierre, *J. Mater. Chem. B*, 2013, **1**, 2818–2828.
21 R. H. Kodama, *J. Magn. Magn. Mater.*, 2009, **200**, 359–372.
22 G. Wang, X. Zhang, A. Skallberg, Y. Liu, Z. Hu, X. Mei and K. Uvdal, *Nanoscale*, 2014, **6**, 2953–2963.
23 U. I. Tromsdorf, O. T. Bruns, S. C. Salmen, U. Beisiegel and H. Weller, *Nano Lett.*, 2009, **9**, 4434–4440.
24 J. P. Finn, K.-L. Nguyen, F. Hana, Z. Zhou, I. Salusky, I. Ayada and P. Hu, *Clin. Radiol.*, 2016, **71**, 796–806.
25 J. Huang, L. Wang, X. Zhong, Y. Li, L. Yang and H. Mao, *J. Mater. Chem. B*, 2014, **2**, 5344–5351.
26 D. Ling and T. Hyeon, *Small*, 2013, **9**, 1450–1466.
27 B. H. Kim, N. Lee, H. Kim, K. An, Y. I. Park, Y. Choi, K. Shin, Y. Lee, S. G. Kwon, H. B. Na, J.-G. Park, E.-Y. Ahn, Y.-W. Kim, W. K. Moon, S. H. Choi and T. Hyeon, *J. Am. Chem. Soc.*, 2011, **133**, 12624–12631.
28 Y.-P. Rui, B. Liang, F. Hu, J. Xu, Y.-F. Peng, P.-H. Yin, Y. Duan, C. Zhang and H. Gu, *RSC Adv.*, 2016, **6**, 22575–22585.
29 G. L. Ellman, K. D. Courtney, V. Andres Jr and R. M. Featherstone, *Biochem. Pharmacol.*, 1961, **7**, 88–95.
30 M. L. Hu, *Methods Enzymol.*, 1994, **233**, 380–385.

31 S. Sudipta Chakraborty, K. S. Sharma, A. Rajeswari, K. V. Vimalnath, H. D. Sarma, U. Pandey, Jagannath, R. S. Ningthoujam, R. K. Vatsa and A. Dash, *J. Mater. Chem. B*, 2015, **3**, 5455–5466.
32 D. Cheng, D. Li, C. Zhang, H. Tan, C. Wang, L. Pang and H. Shi, *ACS Appl. Mater. Interfaces*, 2015, **7**, 2847.
33 Y. Yang, L. Zhang, J. Cai, X. Li, D. Cheng, H. Su, J. Zhang, S. Liu, H. Shi and Y. Zhang, *ACS Appl. Mater. Interfaces*, 2016, **8**, 1525–1531.
34 C. Zhang, X. Xie, S. Liang, M. Li, Y. Liu and H. Gu, *Nanomedicine: Nanotechnology, Biology and Medicine*, 2011, **8**, 996–1006.
35 M. Irigoyen, M. J. Pajares, J. Agorreta, M. P. Ponz-Sarvisé, E. Salvo and M. D. Lozano, *Mol. Cancer*, 2010, **9**, 130–142.
36 S. Xue, C. Zhang, Y. Yang, L. Zhang, D. Cheng, J. Zhang, H. Shi and Y. Zhang, *J. Biomed. Nanotechnol.*, 2015, **11**, 1027.
37 G. H. Simon, J. Bauer, O. Saborovski, Y. Fu, C. Corot, M. F. Wendland and H. E. Daldrup-Link, *Eur. J. Radiol.*, 2006, **16**, 738–745.
38 E. Peng, F. Wang and J. M. Xue, *J. Mater. Chem. B*, 2015, **3**, 2241–2276.
39 M. Li, H. Gu and C. Zhang, *Nanoscale Res. Lett.*, 2012, **7**, 204.
40 L. Xiao, J. Li, D. F. Brougham, E. K. Fox, N. Feliu, A. Bushmelev, A. Schmidt, N. Mertens, F. Kiessling, M. Valldor, B. Fadeel and S. Mathur, *ACS Nano*, 2011, **5**, 6315–6324.
41 M. Taupitz, J. Schnorr, C. Abramjuk, S. Wagner, H. Pilgrimm, H. Hunigen and B. Hamm, *J. Magn. Reson. Imag.*, 2000, **12**, 905–911.
42 L. Wang, J. Du, Y. Zhou and Y. Wang, *Nanomedicine: Nanotechnology, Biology and Medicine*, 2017, **13**, 455–469.
43 A. Roch, Y. Gossuin, R. N. Muller and P. Gillis, *J. Magn. Magn. Mater.*, 2005, **293**, 532–539.
44 F. Xu, C. Cheng, D.-X. Chen and H. Gu, *ChemPhysChem*, 2012, **13**, 336–341.
45 F. Hu and Y. S. Zhao, *Nanoscale*, 2012, **4**, 6235–6243.
46 L. Calucci, A. Grillone, E. R. Riva, V. Mattoli, G. Ciofani and C. Forte, *J. Phys. Chem. C*, 2017, **121**, 823–829.
47 C. Billotey, C. Wilhelm, M. Devaud, J. C. Bacri, J. Bittoun and F. Gazeau, *Magn. Reson. Med.*, 2003, **49**, 646–654.
48 M. A. Abakumov, N. V. Nukolova, M. Sokolsky-Papkov, S. A. Shein, T. O. Sandalova, H. M. Vishwasrao, N. F. Grinenko, I. L. Gubsky, A. M. Abakumov, A. V. Kabanov and V. P. Chekhonin, *Nanomedicine: Nanotechnology, Biology and Medicine*, 2015, **11**, 825–833.
49 Z. Li, P. W. Yi, Q. Sun, H. Lei, H. L. Zhao, Z. H. Hua Zhu, S. C. Smith, M. B. Lan and G. Q. Lu, *Adv. Funct. Mater.*, 2012, **12**, 2387–2393.
50 S. Y. Lee, S. I. Jeon, S. Jung, I. J. Chung and C.-H. Ahn, *Adv. Drug Delivery Rev.*, 2014, **76**, 60–78.
51 K. Zarschler, L. Rocks, N. Licciardello, L. Boselli, E. Polo, K. P. Garcia, L. D. Colac, H. Stephan and K. A. Dawson, *Nanomedicine: Nanotechnology, Biology and Medicine*, 2016, **12**, 1663–1701.
52 E. Ruoslahti, *Annu. Rev. Cell Dev. Biol.*, 1996, **12**, 697–715.
53 X. Tong, Z. Wang, X. Sun, J. Song, O. Jacobson, G. Niu, D. O. Kiesewetter and X. Chen, *Theranostics*, 2016, **6**, 2039–2051.